Construction and Building Materials 541 (2026) 147801

Contents lists available at ScienceDirect

Construction and Building Materials

journal homepage: www.elsevier.com/locate/conbuildmat

A study on the corrosion resistance of magnesium potassium phosphate cement coatings with surface hydrophobic treatment by HDTMS

Xiong Xie [a,b], Tingyu Xiang [a,b], Danqian Wang [a,b,*], Jinyang Jiang [a,b]

[a] School of Materials Science and Engineering, Southeast University, Nanjing 211189, China
[b] State Key Laboratory of Engineering Materials for Major Infrastructure, Southeast University, Nanjing 211189, China

ARTICLE INFO

Keywords:
Magnesium potassium phosphate cement
Coatings
Hydrophobic treatment
Hydrophobicity
Corrosion resistance

ABSTRACT

Magnesium potassium phosphate cement (MKPC) coatings exhibit excellent bonding properties and environmental friendliness. However, as an inorganic coating, MKPC coatings exhibit poor impermeability. This study utilized hexadecyltrimethoxysilane (HDTMS), $CaCl_2$ and $NaHCO_3$ to achieve hydrophobic treatment of the MKPC coating surface. Effects of hydrophobic treatment on the properties of the coating and substrate were characterized by various tests, and mechanisms of corrosion resistance were explored. The results indicate that reducing the surface energy of the coating by HDTMS can improve hydrophobicity of the coating, and increasing the surface roughness by generating $CaCO_3$ can further enhance the hydrophobicity. Surface treatment enables the coating to maintain prolonged hydrophobicity in a 3.5% NaCl solution. Meanwhile, hydrophobic treatment inhibits the formation of hazenite, enhances the permeability resistance of MKPC, and can provide a long-term improvement in the corrosion resistance for low carbon steel, the best sample exhibited a corrosion current density that was one-third that of the untreated sample after 28 d of immersion.

1. Introduction

Steel is widely used in various types of infrastructure due to its outstanding properties. However, when exposed to harsh environments such as seawater, corrosion often poses a safety risk and results in significant financial losses. Statistically, the direct economic losses from corrosion amount to trillions of dollars a year [1,2]. Therefore, it is important to improve the corrosion resistance of steel. Current common methods of corrosion protection include modifying the composition of steel and treating steel surface, of which applying an anti-corrosion coating directly to the surface is the easiest and most cost-effective way to prevent corrosion [3].

Anti-corrosion coatings generally consist of organic and inorganic coatings. While traditional organic coatings, such as epoxy resins, polyurethanes, etc., provide strong adhesion, shortcomings include susceptibility to aging, poor heat resistance, and potential release of harmful substances that severely limit durability [4–6]. In contrast, inorganic phosphate-based composite coatings present a significant avenue for development as new coating materials, due to the superior corrosion resistance, high temperature stability, and environmentally friendly properties [7].

Magnesium phosphate cement (MPC) is an inorganic binder formed by an acid-base reaction between dead-burned magnesium oxide (MgO), phosphate, and a retarder. Common phosphates include ammonium dihydrogen phosphate ($NH_4H_2PO_4$) and potassium dihydrogen phosphate (KH_2PO_4), which can be used to prepare magnesium ammonium phosphate cement (MAPC) and magnesium potassium phosphate cement (MKPC), respectively [8]. It has the potential to be used as an inorganic anti-corrosion coating due to its strong adhesion, high early strength, excellent volume stability, corrosion resistance, and ability to form a protective film on the surface of reinforcing bars [8–10]. However, inorganic materials have limited impermeability, which adversely affects the long-term corrosion resistance [11–14], so improving the impermeability of MPC coatings is essential for its suitability as a corrosion resistant coating.

Hydrophobic treatment can effectively reduce the negative effects of water or corrosion solutions on cement-based coatings; applying hydrophobic treatment to MKPC coatings is a critical approach to enhance the impermeability [9]. Hydrophobic treatments are mainly classified into bulk modification and surface treatment. It is important to note that bulk modifications tend to damage the internal structure, leading to a decrease in properties such as strength [15–17]. Meanwhile, surface

* Corresponding author at: School of Materials Science and Engineering, Southeast University, Nanjing 211189, China.
E-mail addresses: xiexiong000120@163.com (X. Xie), tingyu.xiang@seu.edu.cn (T. Xiang), danqian.wang@seu.edu.cn (D. Wang), jiangjinyang16@163.com (J. Jiang).

https://doi.org/10.1016/j.conbuildmat.2026.147801
Received 27 May 2026; Received in revised form 24 July 2026; Accepted 12 August 2026
Available online 19 August 2026

Table 1
Oxide composition of dead burned MgO (wt%).

MgO	SiO_2	CaO	Fe_2O_3	Al_2O_3
97.5	0.50	1.10	0.65	0.15

Table 2
MKPC mixing ratio (g).

MgO	KH_2PO_4	Borax	H_2O
50	34	5	16.8

Table 3
Ratios of surface treatment solutions (ml).

	HDTMS	HDTMS-$CaCl_2$	$NaHCO_3$	H_2O
Control	/	/	/	/
HDTMS	90	/	/	30
HDTMS + $CaCl_2$	/	90	/	30
HDTMS + $NaHCO_3$	90	/	30	/
HDTMS + $CaCl_2$ + $NaHCO_3$	/	90	30	/

treatment only affects the surface of the coating and has little impact on the overall structure [18,19]. At present, there has been considerable research into the surface treatment of ordinary portland cement [20–22], but little research has been conducted on MKPC. Traditional treatment involves directly adsorbing a layer of low surface energy molecules onto the surface; however, the hydrophobicity are limited by initial surface roughness, and the durability of the hydrophobic layer is limited [23]. By restructuring the surface layer in terms of both structure and composition, it is possible to simultaneously enhance both hydrophobicity and durability [18]. Therefore, it is essential to investigate the impact of surface hydrophobic treatment on MKPC coatings by analyzing the effect on the impermeability and corrosion resistance of the coating.

This study uses HDTMS to treat the MKPC coatings, calcium chloride dihydrate ($CaCl_2·2H_2O$) and sodium bicarbonate ($NaHCO_3$) are also used to increase surface roughness (the two react to form $CaCO_3$). The influence of different combinations on the hydrophobicity and corrosion resistance by contact angle testing and various electrochemical testing methods (OCP, LPR, EIS, and Tafel). At the same time, various testing methods, including mass change testing, SEM, XRD, Raman spectroscopy and MIP, were utilized to analyze the changes in samples with different surface treatments before and after immersion in a 3.5 wt% NaCl solution, thereby further elucidating the mechanism by which the hydrophobic MKPC coating inhibits corrosion in low carbon steel.

2. Materials and methods

2.1. Raw materials

This study used cold rolled Q235 low carbon steel with dimensions of 10 × 10 × 3 mm. Dead burned MgO was produced by calcination at 1650 ℃ and has a purity of approximately 97%, the composition is shown in Table 1. KH_2PO_4 (AR, >99.5%), borax ($Na_2B_4O_7·10\,H_2O$, AR, >99.5%, as a retarder), HDTMS (GC, ≥85%), $CaCl_2·2H_2O$ (AR, >99%), and $NaHCO_3$ (AR, >99.8%) were all purchased from Shanghai Aladdin Biochemical Technology Co., Ltd. All water used in the experiments was deionized water.

2.2. Treatment of low carbon steel and preparation of MKPC coatings

The low carbon steel is first treated with a 5% NaOH solution and a 5% H_2SO_4 solution to remove grease and rust. Subsequently, the steel is polished with 80, 220, and 600 mesh sandpaper in sequence, then placed in ethanol for ultrasonic cleaning for 10 min, and finally dried for storage.

The composition of the MKPC coating is shown in Table 2, with an M/P ratio of 5 (molar ratio), a w/c ratio of 0.2, and borax accounting to 10% of the mass in MgO. The detailed preparation process is as follows:

- Firstly, the specified quantities of KH_2PO_4 and borax were dissolved in deionized water and stirred for 2 min;
- Then MgO was added and stirred for 2 min to obtain a fresh paste;
- Finally, the paste was poured into moulds containing steel sheets (each mould measuring 10 × 10 × 5 mm, the MKPC coating thickness is 2 mm), cured for 7 d at 20 ± 2 ℃ and 65 ± 5% RH, followed by surface hydrophobic treatment.

2.3. Surface hydrophobic treatment

In this study, four sets of surface treatment experiments were designed, where the MKPC was treated by heating and soaking. an

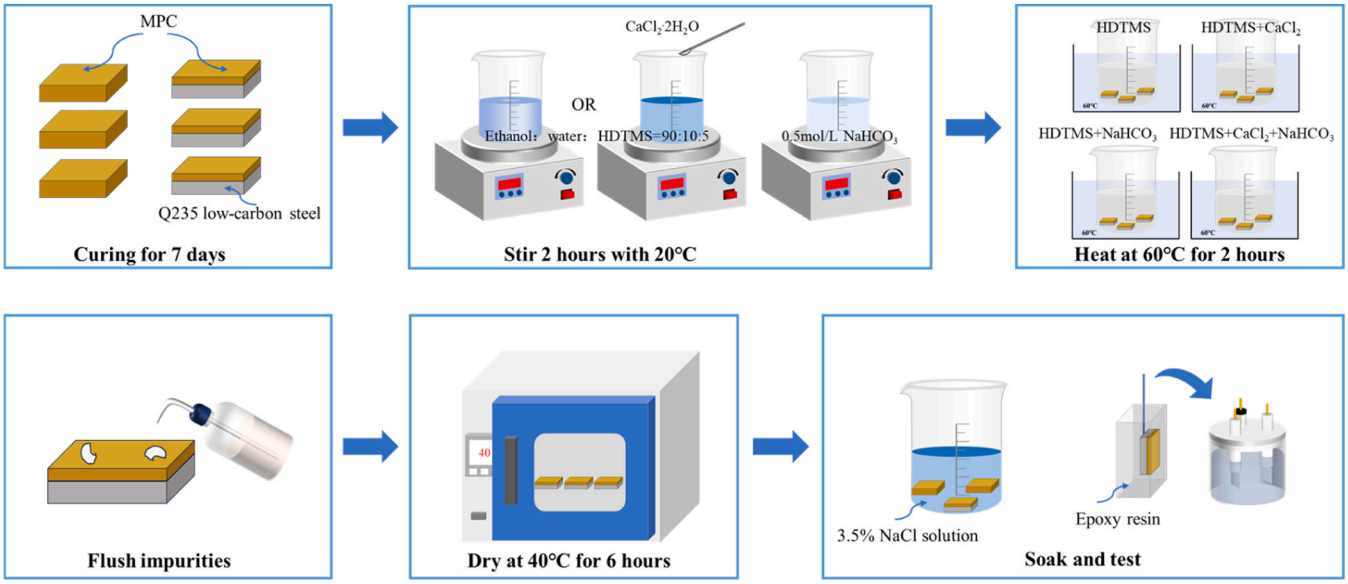

Fig. 1. Sample preparation flowchart.

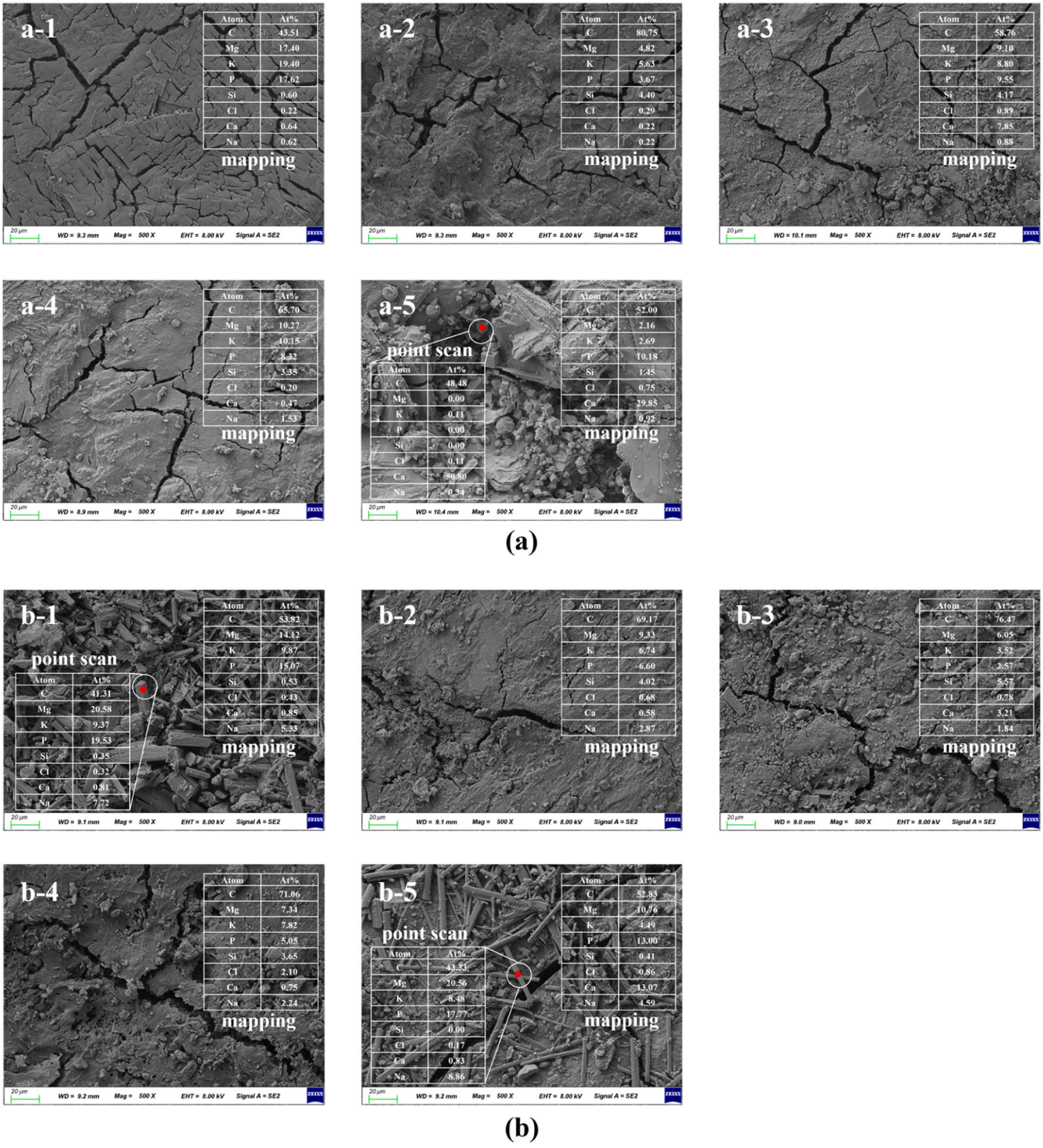

Fig. 2. SEM-EDS of MKPC samples with different soaking time: (a) 0d (a−1 Control; a−2 HDTMS; a−3 HDTMS+$CaCl_2$; a−4 HDTMS+$NaHCO_3$; a−5 HDTMS+$CaCl_2$+$NaHCO_3$); (b)28d (b−1 Control; b−2 HDTMS; b−3 HDTMS+$CaCl_2$; b−4 HDTMS+$NaHCO_3$; b−5 HDTMS+$CaCl_2$+$NaHCO_3$).

HDTMS hydrolytic solution was prepared by mixing ethanol, water and HDTMS in a volume ratio of 90:10:5. At the same time, a solution was prepared by adding $CaCl_2{\cdot}2H_2O$ to the same mixture to form a 0.5 mol/L HDTMS–$CaCl_2$ solution. Both solutions were stirred at 20 ± 2 ℃ for 2 h. In addition, an aqueous solution of $NaHCO_3$ with a concentration of 0.5 mol/L was prepared. The specific process is as follows:

- Firstly, place the coating samples in a beaker, add the appropriate volumes of solution as specified in Table 3;
- Secondly, place the beaker in a water bath, heat at 60°C for 2 h, then flush the surface with deionized water and ethanol until no visible impurities;
- Finally, dry in a vacuum oven at 40 ℃ for 6 h to complete the hydrophobic surface treatment. The flowchart of the process is shown in Fig. 1.

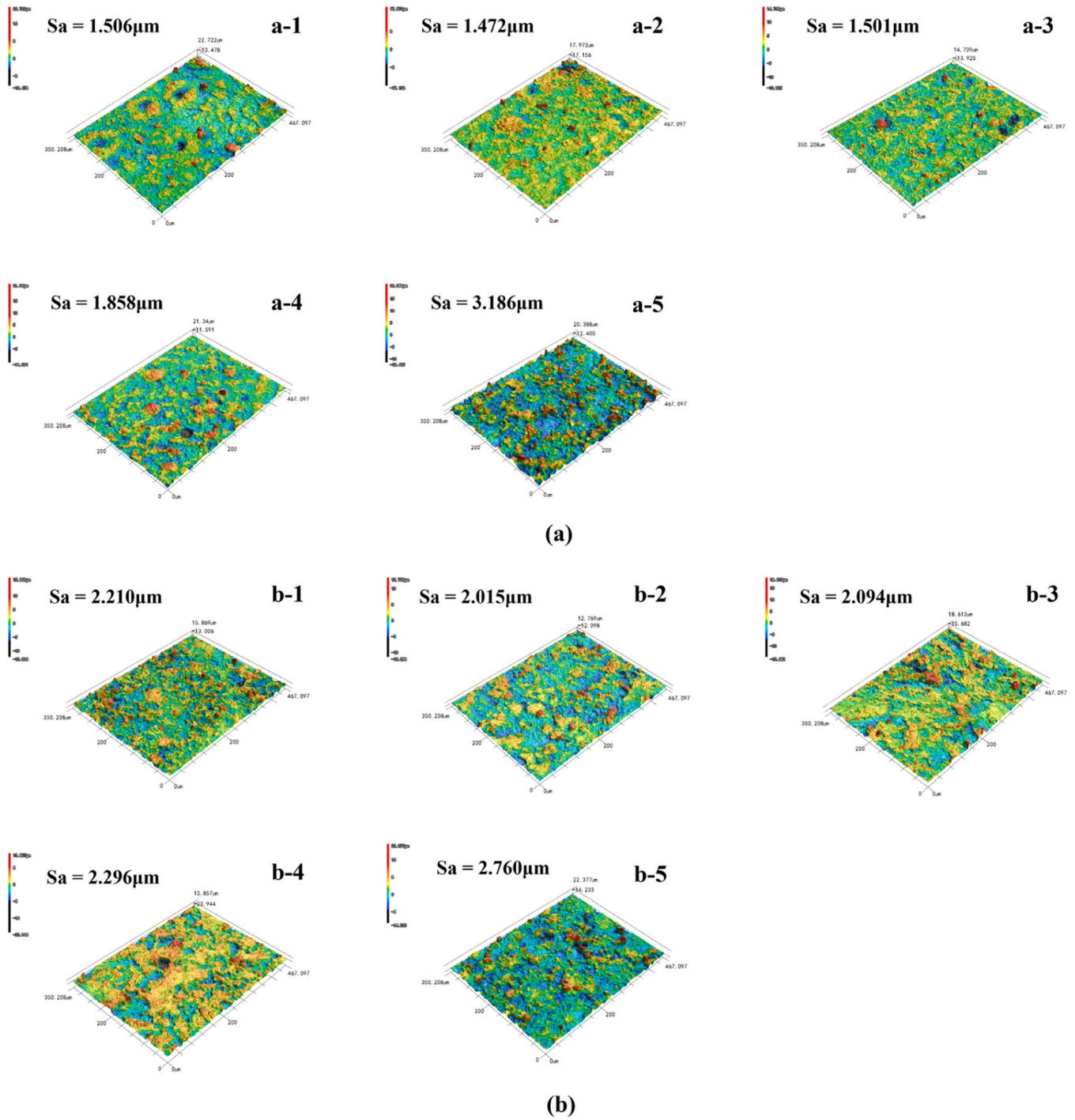

Fig. 3. Images of 3D rough structures of MKPC samples with different soaking times: (a) 0d (a−1 Control; a−2 HDTMS; a−3 HDTMS+$CaCl_2$; a−4 HDTMS+$NaHCO_3$; a−5 HDTMS+$CaCl_2$+$NaHCO_3$); (b)28d (b−1 Control; b−2 HDTMS; b−3 HDTMS+$CaCl_2$; b−4 HDTMS+$NaHCO_3$; b−5 HDTMS+$CaCl_2$+$NaHCO_3$).

2.4. Test method

Following the electrochemical tests, all other samples were subjected to stop hydration treatment before testing. The specific process involves: soaking the samples in ethanol for 48 h, then drying in a vacuum oven at 40°C for 48 h, after which the process is complete.

2.4.1. Electrochemical testing

Electrochemical testing was carried out using a CS2350M potentiostat (Corrtest, China) in a 3.5 wt% NaCl solution, with test durations from 2 h to 28 d (2 h, 1d, 3d, 7d, 14d, and 28d). Open circuit potential (OCP) test lasted 600 s. Linear polarization resistance (LPR) was measured within the range of −0.015 V_{OCP} to 0.015 V_{OCP}, with a scan rate of 0.16 mV/s. Electrochemical impedance spectroscopy (EIS) frequency was scanned from 100 kHz to 0.01 Hz. The EIS data was fitted by ZSimpWin software. Tafel Curve (Tafel) measurement range was from −0.3 V_{OCP} to 1.5 V_{OCP}, with a scan rate of 1 mV/s.

2.4.2. Microstructure

The surface morphology and energy dispersive spectroscopy (EDS) analysis of the coating were tested with a Sigma 560 electron microscope (Zeiss, Germany). Surface structure and roughness measurements

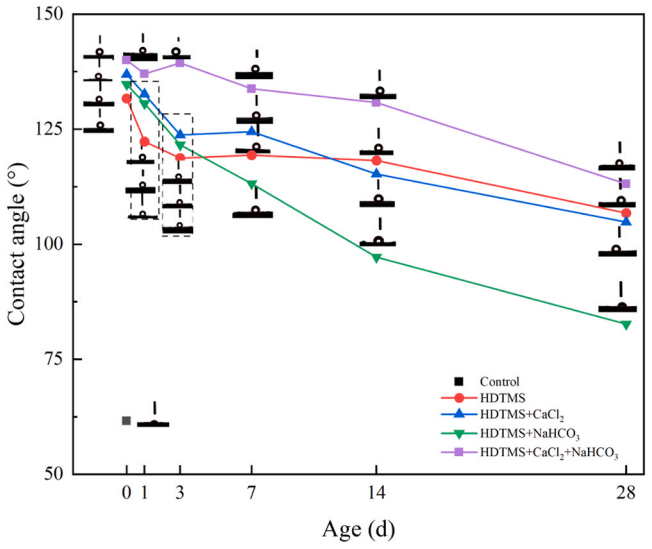

Fig. 4. Contact angles of MKPC specimens.

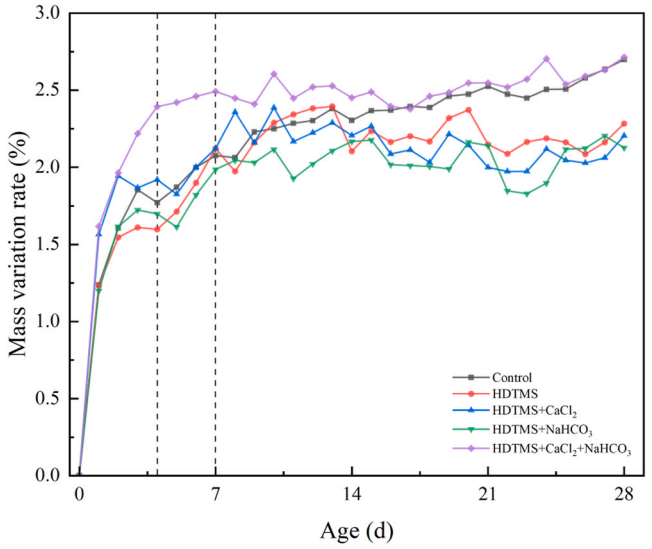

Fig. 5. Weight variation ratio evolution of specimens.

were performed using a VK-X1000 optical profilometer (Keyence, Japan). pore structure was characterized by an Autopore IV 9510 mercury porosimeter (Micromeritics, USA), with a pore size range of 6 nm to 354 μm.

2.4.3. Phase analysis

A D8 X-ray diffractometer (Bruker, Germany) was used to measure the coating surface via grazing-incidence XRD (GIXRD), with a scan range of 10–70°, a scan rate of 5°/min, and a grazing angle of 1°, the test samples were in block form. Raman spectroscopy was performed on the coating surface and the low carbon steel surface with an Xplora Plus micro-Raman spectrometer (Horiba, France), with a laser wavelength of 532 nm.

2.4.4. Contact angle test

Coating contact angle measurements were tested with the LSA 100 (Lauda Scientific, Germany). The test liquid is deionized water, with a volume of 2 μL. A photograph is taken at the moment the droplet stabilizes (typically 0.5–2 s).

2.4.5. Mass variation

Analyze the mass variation of the samples in a 3.5% NaCl solution according to Eq. (1).

$$\Delta m = \frac{m_{final} - m_{initial}}{m_{initial}} \times 100\% \quad (1)$$

In the equation, Δm is the mass variation rate (%), $m_{initial}$ is the mass before soaking (g), and m_{final} is the mass after soaking (g).

3. Results and discussion

3.1. Microstructure and hydrophobicity

Fig. 2 shows the microstructure and elemental composition of five MKPC samples after 0 and 28 d of soaking in 3.5% NaCl solution. It can be observed from Fig. 2(a) that cracks were present on the surface of coatings subjected to treatment with HDTMS, HDTMS + $CaCl_2$ and HDTMS + $NaHCO_3$ solutions, these cracks remain clearly visible, indicating that the immersion in these solutions do not affect the surface structure of coating. Furthermore, the EDS results show that the HDTMS, HDTMS + $CaCl_2$ and HDTMS + $NaHCO_3$ samples contain significant amounts of Si, indicating that HDTMS can effectively bond to the coating surface. Conversely, Fig. 2(a)−5 demonstrates that the HDTMS + $CaCl_2$ + $NaHCO_3$ sample exhibits a much denser surface and fewer cracks, meanwhile distinct cubic crystals were present. Corresponding EDS result indicates that $CaCO_3$ crystals have formed on the surface of HDTMS + $CaCl_2$ + $NaHCO_3$ sample, mainly through the reaction between $CaCl_2$ and $NaHCO_3$, which markedly enhances the surface roughness of MKPC coating.

Figs. 2(b)-1 shows the microstructure of the Control sample after 28 d soaking. Compared with the unsoaked sample, the surface was denser and covered with acicular crystals. which is consistent with the study by Wang et al. [3]. The EDS result shows that the composition mainly includes P, Mg, K, and Na, which may be related to the transformation of K-struvite into hazenite in NaCl solution [24,25]. However, as shown in Figs. 2(b)−2 and 2b−3, only a minor amount of crystals could be observed in the HDTMS and HDTMS + $CaCl_2$ samples, which causes a lower degree of microstructural density than the Control sample. This may be due to the hydrophobicity of the surface inhibiting the reaction between NaCl and K-struvite, resulting in limited formation of hazenite. Furthermore, HDTMS and HDTMS + $CaCl_2$ samples still contained Si, indicating that some HDTMS remained bound to the surface even after prolonged soaking. The surface struture of HDTMS + $NaHCO_3$ sample was similar to the HDTMS and HDTMS + $CaCl_2$ samples, except that small crystals were distributed in some areas. Fig. 2(b)−5 illustrates that, after prolonged soaking, both $CaCO_3$ and hazenite were present on the sample surface, and the quantity was fewer than the Control sample, this may be because the fine $CaCO_3$ crystals act as nucleation sites, facilitating the growth of hazenite.

Fig. 3 presents the surface roughness results for five MKPC samples. These results match the SEM results in Fig. 2. As shown in Fig. 3(a), the surface of HDTMS + $CaCl_2$ + $NaHCO_3$ sample was rougher than other four groups before soaking. This is because $CaCl_2$ reacts with $NaHCO_3$ to form micron-sized $CaCO_3$, these particles bind to the surface and increase roughness. After soaking for 28 d, the surface roughness of the Control, HDTMS, HDTMS + $CaCl_2$, and HDTMS + $NaHCO_3$ samples increased, particularly in the Control sample. In contrast, the HDTMS + $CaCl_2$ + $NaHCO_3$ sample showed decreased roughness, as shown in Figs. 3(b)-5. The difference between HDTMS + $CaCl_2$ + $NaHCO_3$ sample and the other samples could be

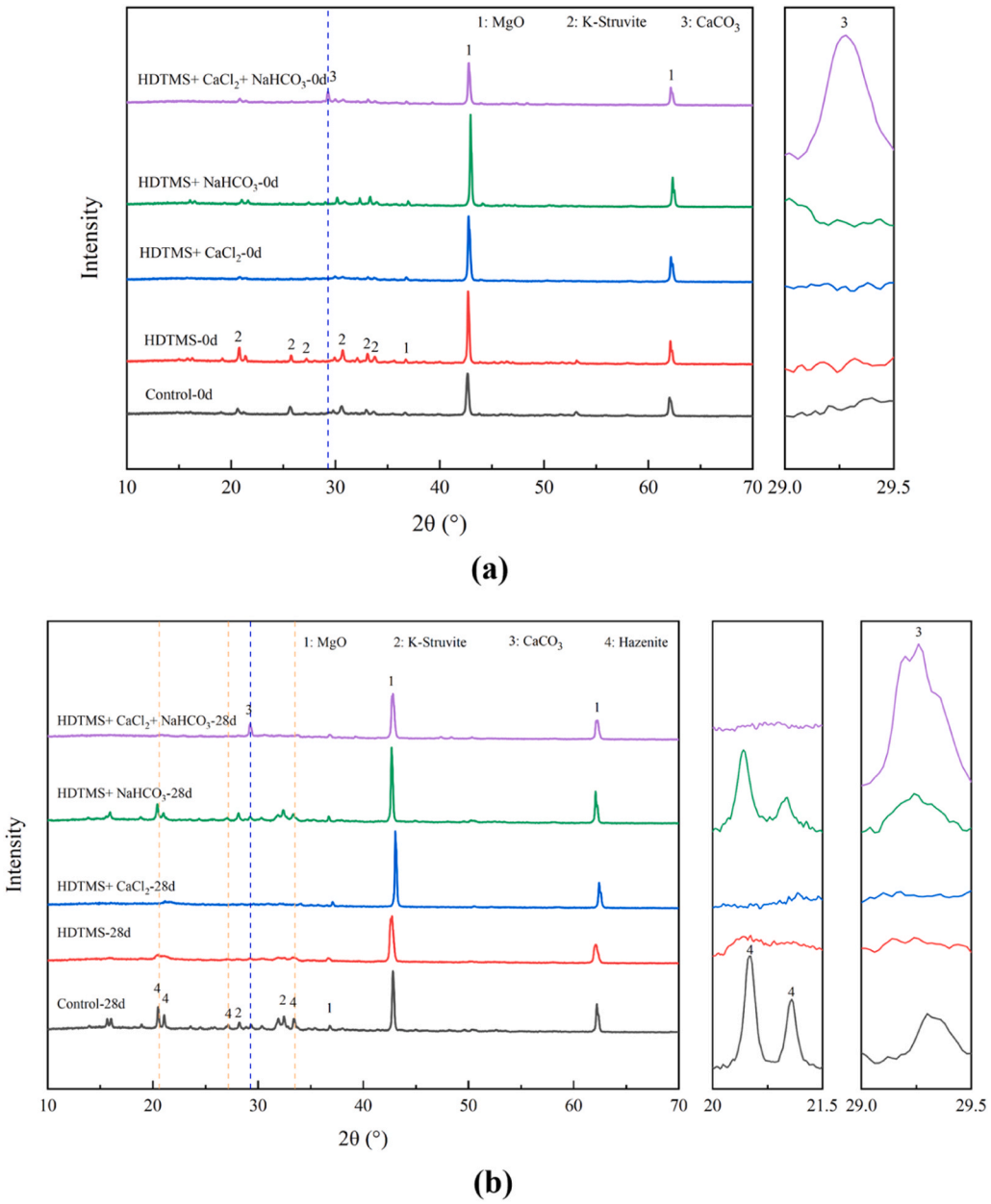

Fig. 6. GIXRD of MKPC with different soaking time: (a) 0d; (b)28d.

explained by the formation of new phases, which may increase surface density and alter the microstructure, resulting in less surface roughness. According to the Wenzel and Cassie-Baxter wetting models, surface roughness significantly influence the contact angle of a surface. This provides the basis for the contact angle results presented later [26].

Fig. 4 presents the contact angle results for four hydrophobically treated MKPC samples after soaking in a 3.5% NaCl solution. Prior to soaking, the contact angle of the Control sample was 61.6° , which is indicative of its hydrophilic properties. In contrast, the contact angles of all four treated samples were exceeded 130°, demonstrating that each composition ratio successfully enhanced the hydrophobicity of MKPC. Among these, the HDTMS + $CaCl_2$ + $NaHCO_3$ sample achieved the highest contact angle of 140°, which is attributed to the combined effect of HDTMS and greater roughness on the sample surface. As the soaking time increases, the contact angle of the hydrophobic samples in each group gradually decreases. The HDTMS and HDTMS + $CaCl_2$ samples exhibited similar evolution of contact angles, with the contact angles reduced from 131.7° and 136.9° to 106.8° and 104.8° respectively at 28 d. In contrast, the HDTMS + $NaHCO_3$ sample exhibited a more significant decrease, dropping from 134.8 to 82.7°at 28 d, corresponding to a decrease of 38.7%, thus losing the hydrophobicity. As previously mentioned, during the soak process, new phase may continuously forms and adheres to the surface, which may contribute to the observed decrease in hydrophobicity at 28 d. Additionally, factors such as the loss of low surface energy substances [27] and the disappearance of the air layer on hydrophobic surfaces [28] can also result in diminished hydrophobicity. The HDTMS + $CaCl_2$ + $NaHCO_3$ sample displayed the smallest change prior to 14 d, with a reduction to only 130.8°, and stood at 113.1° at 28 d, preserving the best hydrophobic properties among all groups. Notably, the contact angle for the sample showed almost no decline after 3 d of soaking. This is because the surface hydrophobicity is influenced by both low surface energy materials and surface roughness. However, neither of which undergo significant changes during the early soaking stages.

Fig. 5 illustrates the variation in mass of five groups of samples in a 3.5% NaCl solution. The mass of the Control sample steadily increased

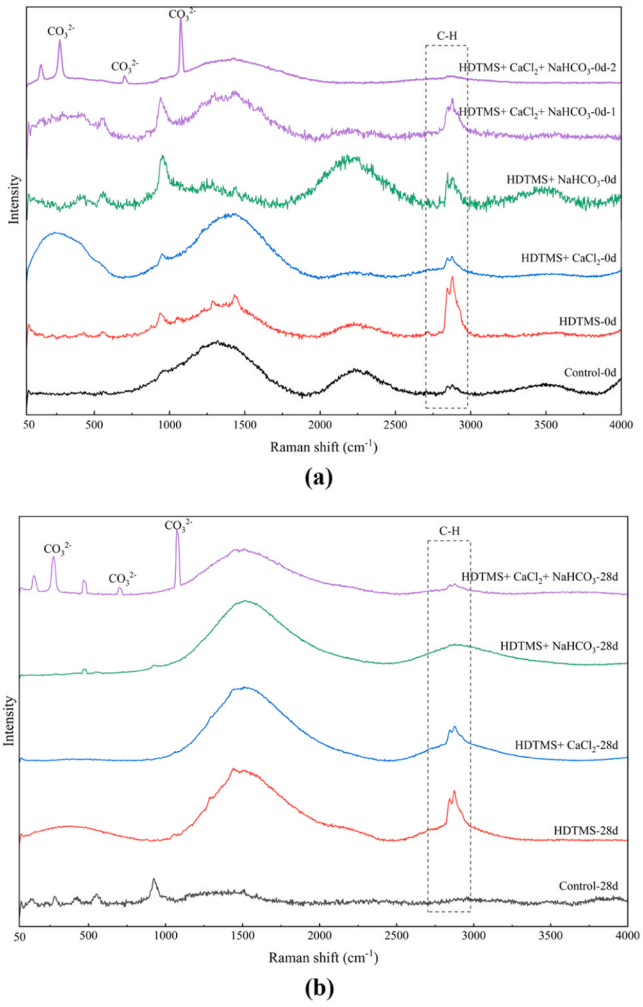

Fig. 7. Raman of MKPC with different soaking time: (a) 0d; (b)28d.

over time, culminating in a 2.7% mass gain after 28 d. This increase was attributed to the continuous formation of hazenite from K-struvite. For the HDTMS, HDTMS + $CaCl_2$, and HDTMS + $NaHCO_3$ samples, the mass increased rapidly during the first 7 d, with mass gain rates of 2.1%, 2.1%, and 1.9%, respectively, followed by stabilization until 28 d. The HDTMS + $CaCl_2$ + $NaHCO_3$ sample exhibited a slower growth rate after 4 d, but the weight gain of sample was greater than other three hydrophobic groups. This is because the sample was more susceptible to forming hazenite compared to others (Figs. 2b-5).

3.2. Composition of phases

Fig. 6 shows the GIXRD results for the five groups of samples before and after soaking, to evaluate the phase composition of the coating surface. As shown in Fig. 6(a), the hydrophobic modification did not alter the types of hydration products. Before soaking, the XRD patterns of all samples exhibits the diffraction peaks corresponding to K-struvite. In comparison, for the HDTMS + $CaCl_2$ + $NaHCO_3$ sample, apart from K-struvite, the diffraction peak assigned to $CaCO_3$ was detected, which resulted from the reaction between $CaCl_2$ and $NaHCO_3$. Fig. 6(b) shows the results after the samples were soaked. hazenite was observed in both the in the Control and HDTMS + $NaHCO_3$ samples, with characteristic diffraction peaks at 2θ values of 20.620°, 21.199°, 27.301° and 33.526° [25]. The HDTMS + $NaHCO_3$ sample lost its hydrophobicity after 28 d, allowing K-struvite to be leached out and converted into hazenite. Meanwhile, $CaCO_3$ remained in the HDTMS + $CaCl_2$ + $NaHCO_3$ sample even after 28 d of soaking, consistent with the SEM results that indicate $CaCO_3$ does not detach during the soaking process.

Fig. 7 shows the Raman spectroscopy results for the five groups of samples. Referring to Fig. 7(a), prior to soaking, all hydrophobic samples exhibited distinct characteristic peaks at 2800–3000 cm^{-1} , which corresponds to the symmetric and asymmetric stretching vibrations of the methyl (-CH_3) and methylene (-CH_2-) in HDTMS [29]. This finding indicates that the hydrophobic treatment method was effective in grafting silane onto the MKPC surface. In addition, the $CaCO_3$ (CO_3^{2-}) was detected in the HDTMS + $CaCl_2$ + $NaHCO_3$ sample (at 1086, 713 and 284 cm^{-1}) [30]. It is worth noting that, as shown by the two corresponding curves for the HDTMS + $CaCl_2$ + $NaHCO_3$ sample, very little HDTMS adheres to the surface of the $CaCO_3$. This observation aligns with the EDS results, which indicate that the formation of $CaCO_3$ mainly increases surface roughness. Furthermore, HDTMS adsorbs onto the sample surface, reducing surface energy. The combination of these two factors consequently enhances the hydrophobicity of the HDTMS + $CaCl_2$ + $NaHCO_3$ sample. Fig. 7(b) shows the results after the samples had been soaked for 28d. The HDTMS and HDTMS + $CaCl_2$ groups still exhibited distinct HDTMS peaks. In contrast, the HDTMS + $NaHCO_3$ sample showed no such peaks, which corresponds with the contact angle results. This indicates that during the soaking process, the HDTMS either detached from the coating or was covered by other products, thereby causing the HDTMS + $NaHCO_3$ sample to lose the hydrophobicity. Meanwhile, the HDTMS + $CaCl_2$ + $NaHCO_3$ sample still exhibited a distinct CO_3^{2-} characteristic peak after 28d, indicating that $CaCO_3$ does not detach during the soak process. In addition, the presence of HDTMS was detected on the surface, which serves as evidence of its continued hydrophobicity at late times.

3.3. Pore distribution

Fig. 8 shows the MIP results for the five MKPC samples. As illustrated in Figs. 8(a) and 8(c), the porosity of the five groups of samples was concentrated between 24% and 28% before soaking, with the most accessible pore size distributed in the 50–100 nm range. However, after the sample has been soaked for 28 d, the porosity decreases to varying extents, and the most accessible pore sizes shifted significantly to the left, falling in the 30–40 nm range (Fig. 8b). Among these, the Control, HDTMS + $NaHCO_3$ and HDTMS + $CaCl_2$ + $NaHCO_3$ samples exhibited the most significant decrease in porosity, whilst the HDTMS and HDTMS + $CaCl_2$ samples showed only minor reductions of 1.45% and 2.54% respectively. This is consistent with the SEM results (Fig. 2b); suggesting that the decrease in porosity may be due to the continued formation of the product hazenite, which fills the pores. This finding also aligns with the previous research [25].

3.4. Electrochemical testing

Fig. 9 shows the variation in OCP of five MKPC samples after soaking in a 3.5% NaCl solution from 2 h to 28 d. In the Control sample, the OCP decreased to −0.435 V_{SCE} after 1d, which is attributed to the ongoing erosion caused by Cl^-. Subsequently, the OCP showed a fluctuating trend, indicating the formation of corrosion products on the steel surface. In contrast, the OCP for the HDTMS, HDTMS + $CaCl_2$, and HDTMS + $NaHCO_3$ samples demonstrated an upward trend, as the hydrophobicity coatings in HDTMS, HDTMS + $CaCl_2$, and HDTMS + $NaHCO_3$ samples effectively inhibited the erosion of Cl^-. Conversely, the HDTMS + $CaCl_2$ + $NaHCO_3$ sample initially showed a downward trend. Although it demonstrated better hydrophobicity, the

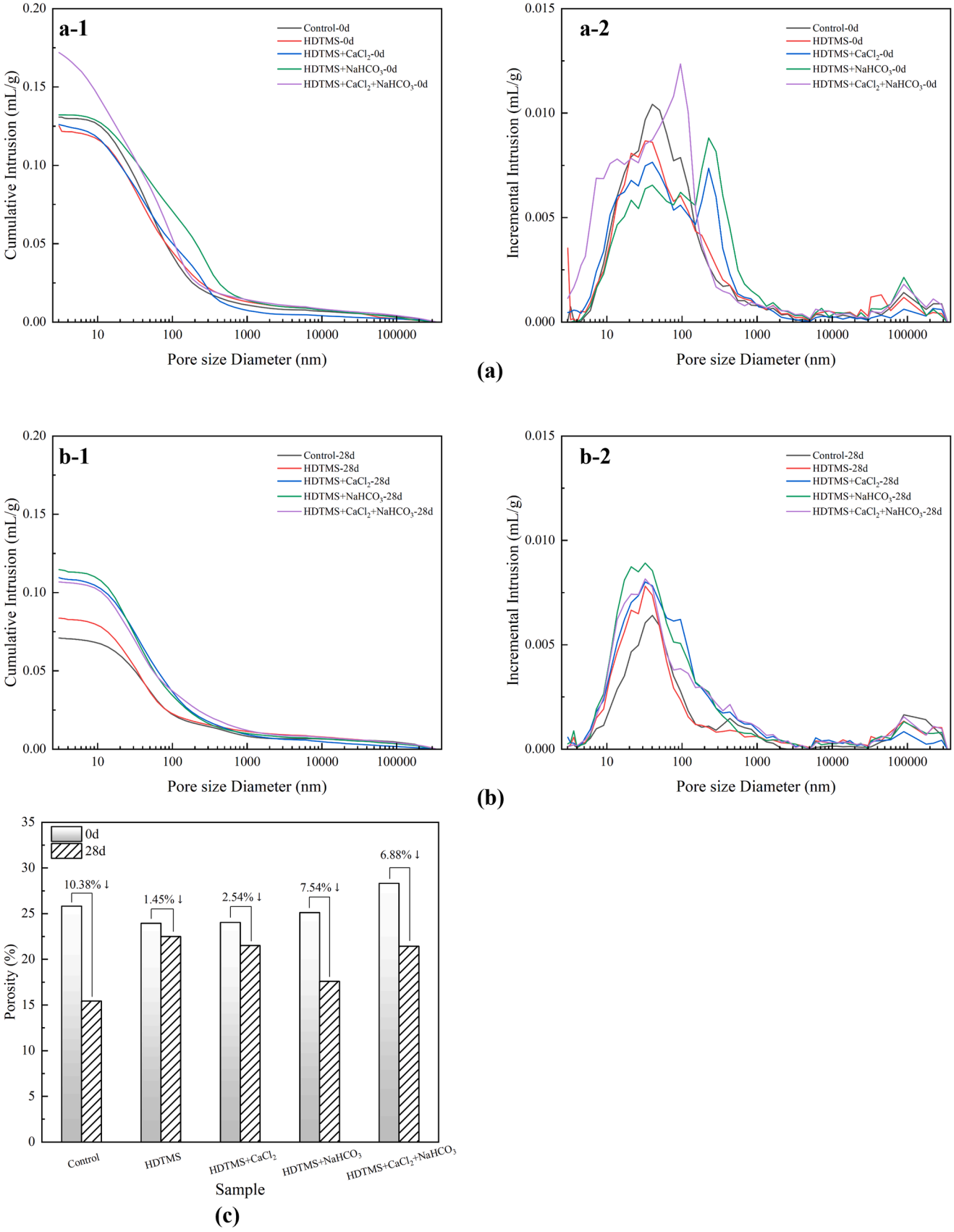

Fig. 8. MIP result of MKPC specimens: (a) 0d; (b)28d; (c) Porosity variation.

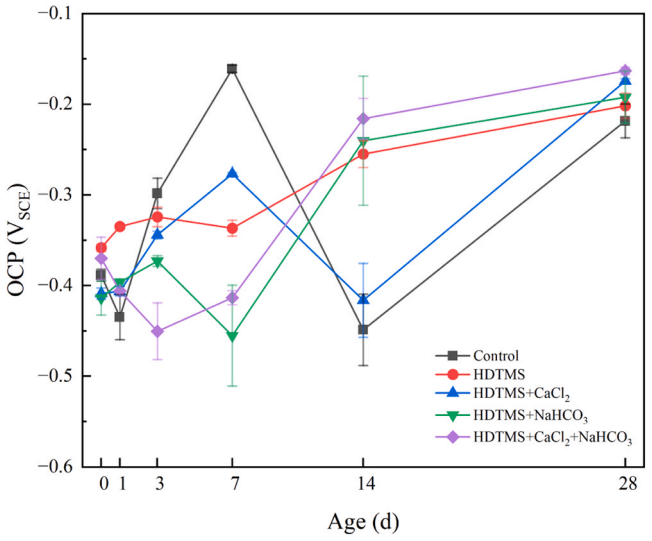

Fig. 9. OCP evolution of different MKPC specimens.

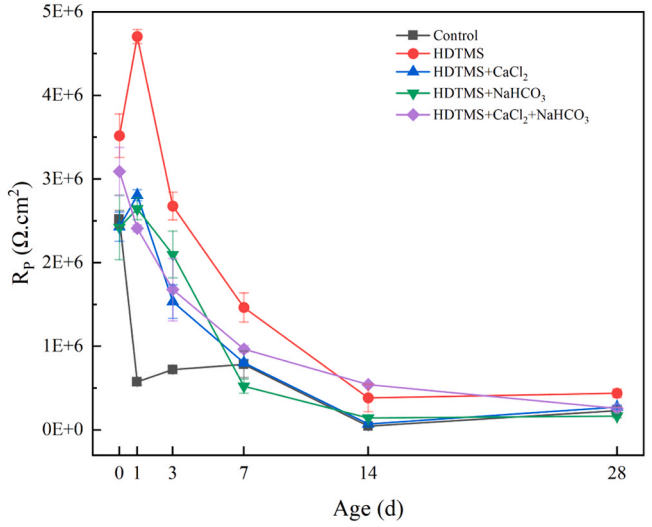

Fig. 10. LPR evolution of different MKPC specimens.

results in Fig. 5 indicate that during the early soaking stages, the surface adsorbs more ions, which increases the risk of corrosion from a thermodynamic. In addition, the surface of the HDTMS + $CaCl_2$ + $NaHCO_3$ group is rougher, this will also affect the OCP. As the soaking period continues, the OCP of the all five samples shows an overall upward trend, likely due to the increased density of the sample. Additionally, the OCP of the hydrophobic samples remains higher than the Control sample, indicating that the hydrophobic treatment of the MKPC surface effectively enhances the corrosion resistance of the substrate over the long term.

Fig. 10 illustrates the LPR results for the five samples. The results show that the data for all samples show a downward trend with increasing soaking time. Notably, the four hydrophobic treatment samples had higher values than the Control sample, especially up to 7 d, suggesting that hydrophobic treatment is beneficial in terms of retardation of substrate corrosion. In the Control sample, the resistance value decreased significantly at 1d; thereafter, the rate of decline slowed, with the resistance value at 28d with 228.8 kΩ. The HDTMS and HDTMS + $CaCl_2$ + $NaHCO_3$ samples exhibited better resistance values at all ages, indicating that these treatments provide excellent corrosion resistance due to the superior hydrophobicity. However, the resistance values of the HDTMS + $CaCl_2$ and HDTMS + $NaHCO_3$ samples were similar to the Control sample at 7d. In the HDTMS + $CaCl_2$ sample, this decline may be related to the addition of Cl^-. Whereas in the HDTMS + $NaHCO_3$ sample, it is likely due to a gradual loss of hydrophobicity, resulting in a reduced ability to inhibit Cl^- corrosion.

To further quantitatively evaluate the effect of the coatings on the corrosion resistance of low carbon steel, Fig. 11 presents the EIS test results for the five samples. As shown in the Nyquist plot in Figs. 11(a)-1, at a soaking time of 2 h, the semicircle diameter in the low frequency range for all hydrophobic treatments exceeded the Control sample, except for the HDTMS + $NaHCO_3$ sample. Fig. 11(b) and (c) show the semicircle diameters in the low frequency range of the Nyquist plot for the Control sample were significantly smaller than the four hydrophobic coatings at 1–3d, indicating that hydrophobic treatment can effectively protect the substrate and inhibit Cl^- corrosion. Furthermore, the HDTMS and HDTMS + $CaCl_2$ samples exhibited superior corrosion resistance, a finding corroborated by the Bode phase angle in the low frequency range. The diameter of the semicircle increases in the low frequency range of the Control sample when the soaking duration is 7d. This may be related to the formation of hazenite, which reduces the porosity of the MKPC coating. As the soaking duration increases further, the semicircular diameter decreases in all samples. However, the samples in the hydrophobic group still performed better than the Control sample. Meanwhile, the Bode phase angle in the low frequency range of the HDTMS + $CaCl_2$ + $NaHCO_3$ sample peaked at 14 and 28 d. This may be due to the enhanced hydrophobicity of the HDTMS + $CaCl_2$ + $NaHCO_3$ sample, which reduce erosion caused by water and Cl^-.

Fig. 12 presents a quantitative analysis of the EIS results, the EIS data were fitted by the equivalent circuit shown in Figs. 12(a) and12(b) [31, 32]. Here, R_s is the solution resistance, R_c and Q_c denote the resistance and capacitance of the MKPC coating respectively, R_f and Q_f indicate the resistance and capacitance of the passive film, and R_{ct} and Q_{dl} represent the charge transfer resistance and capacitance. The fitting error is less than 1×10^{-3}, indicating that the fitted circuit is reasonable. As shown in Fig. 12(c), during the early stages of soaking, the R_c values of all four hydrophobic coatings were higher than the Control. The hydrophobic treatment enhances the impermeability of the MKPC coating, which slows down the dissolution of K-struvite by limiting water penetration. Additionally, the formation of an air film increases the resistance. As soaking time increased, the R_c value in the Control sample began to rise at 3 d, while the other samples also showed an increase in the later stages. This increase in R_c is related to the formation of hazenite and a reduction in porosity. According to Figs. 12d and 12(e), the trends in R_f and R_{ct} are similar. All four hydrophobic coatings showed better results than the Control, further indicating that hydrophobic treatment enhances the corrosion resistance. Notably, the R_{ct} values for the HDTMS, HDTMS + $CaCl_2$, and HDTMS + $CaCl_2$ + $NaHCO_3$ samples remained significantly higher than Control sample after 28 d. This suggests that these three modification methods can withstand corrosive environments over the long term and enhance the corrosion resistance of the substrate.

Fig. 13 depicts the Tafel curves for five samples after 28 d of soaking in a 3.5% NaCl solution; the corrosion potentials and corrosion current densities are shown in Table 4. The corrosion current density is obtained by extrapolation from the Tafel curve of the cathode. As shown in figure, the HDTMS + $CaCl_2$, HDTMS + $NaHCO_3$ and HDTMS + $CaCl_2$ + $NaHCO_3$ samples all exhibit higher corrosion potentials than the Control sample. The HDTMS sample exhibits slightly lower corrosion potentials than the Control. This indicates that the untreated MKPC coating is more susceptible to corrosion, as hydrophobic treatment inhibits the corrosive effects of water and Cl^-, thereby improving the

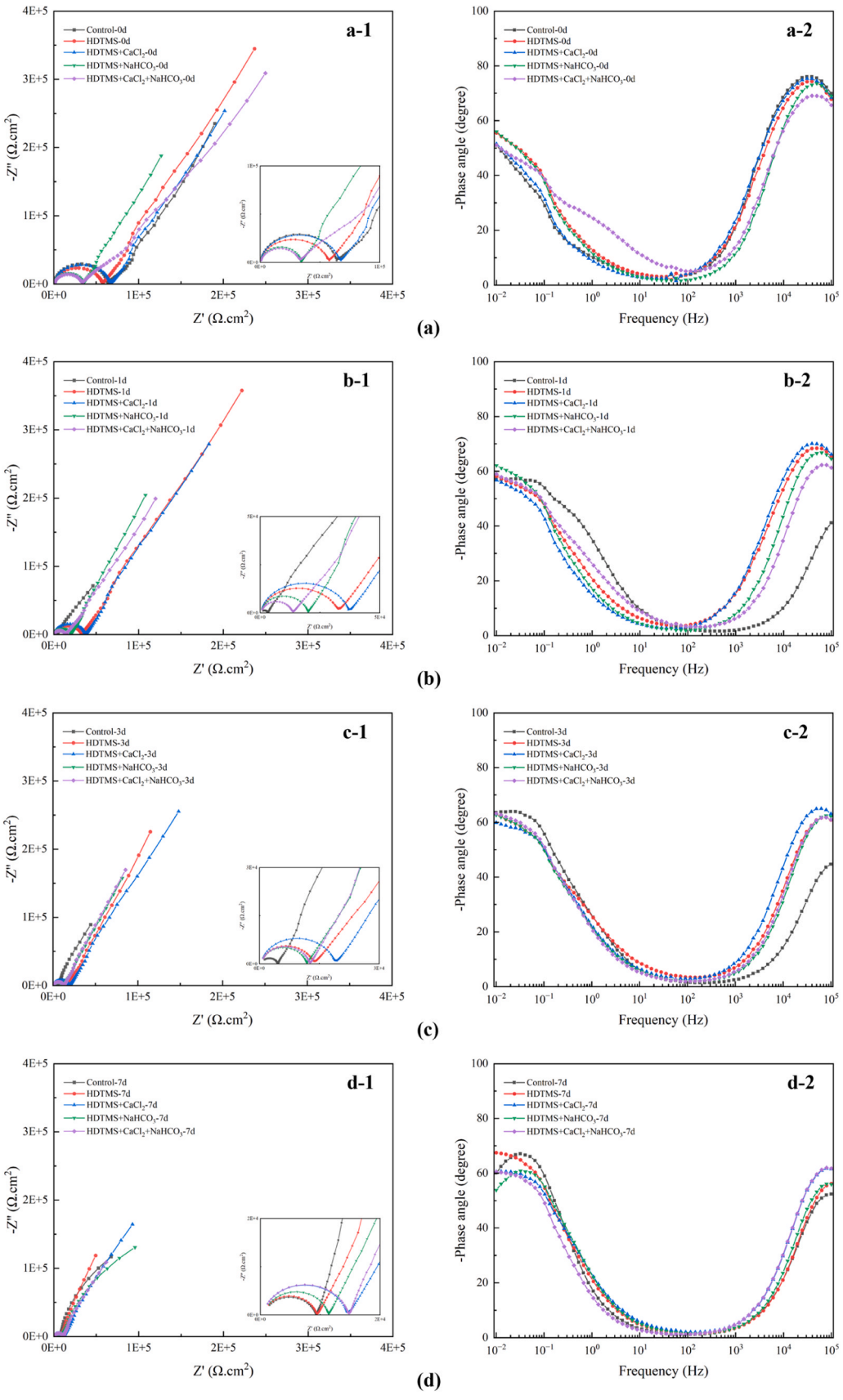

Fig. 11. EIS results of MKPC specimens at different time: (a) 2 h; (b) 1d; (c) 3d; (d) 7d; (e) 14d; (f) 28d.

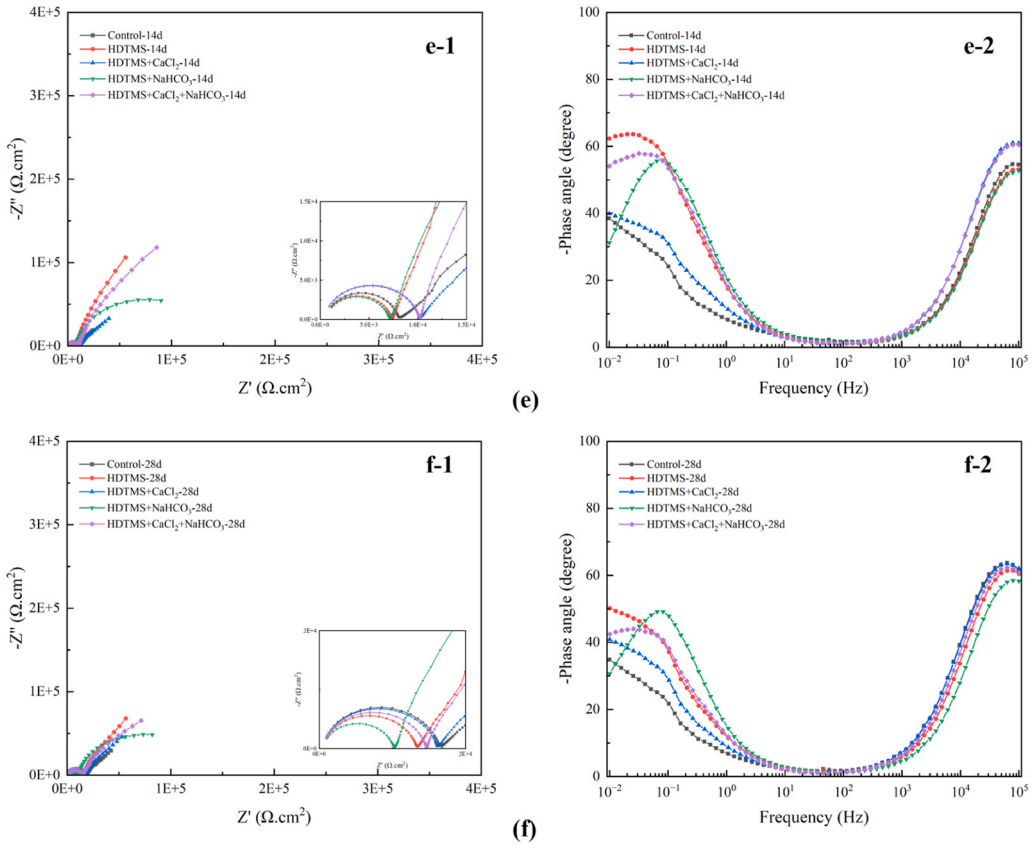

Fig. 11. (*continued*).

corrosion resistance of the substrate. In addition, according to the i_{corr} results, the corrosion current densities of the four hydrated coatings were significantly lower than the Control sample, indicating that the MKPC hydration modification was still effective in inhibiting corrosion of low carbon steel despite the 28d soaking period. Among these, the HDTMS + $CaCl_2$ + $NaHCO_3$ sample exhibited the lowest corrosion current density, demonstrating excellent corrosion resistance.

3.5. Characterisation of steel surface

Fig. 14 shows the Raman spectra of five groups of low carbon steel samples coated with MKPC and immersed in a 3.5% NaCl solution for 28d, additionally, a group of untreated steel samples has been included for reference. The figure shows that the untreated steel samples exhibit a lack of characteristic peaks, whereas the five treated samples display characteristic peaks around 470–485 cm^{-1} ; this corresponds to the Fe-OH asymmetric stretching vibration of α-FeOOH [31,33]. According to the i_{corr} results shown in Fig. 13, the threshold for active corrosion has not been reached, α-FeOOH may be a corrosion product formed at an early stage, and hydrophobic modification does not alter the type of corrosion product.

4. Discussion

As mentioned above, compared with bulk hydrophobic treatment, the surface hydrophobic treatment of MKPC coatings is simple to perform, requiring only soaking in a heated solution, and has minimal impact on the phase composition and pore structure (Figs. 6 and 8). Furthermore, compared with untreated coatings, surface hydrophobic treatment enhances the corrosion resistance of the substrate (Figs. 11, 12 and 13). The effects of surface treatment on hydrophobicity and the mechanism of corrosion resistance are outlined below.

4.1. Mechanisms affecting hydrophobicity via HDTMS and Surface Roughness

The hydrophobicity of materials is often influenced by both chemical composition (surface free energy) and microstructure (roughness) [18]. Generally, materials with lower surface free energy exhibit greater hydrophobicity [26], as a common hydrophobic modifying agent, HDTMS reduces the surface energy of materials and enhances the hydrophobicity [34,35]. Research has shown that silanes hydrolyse to form silanols, which then react through a dehydration condensation process with the hydroxyl groups on the MPKC surface, thereby grafting hydrophobic groups onto the coating surface [36,37]. The results indicate that all four samples treated with HDTMS exhibited hydrophobicity prior to soaking (Fig. 4). As can be seen from Fig. 2(a), the Si content of the HDTMS, HDTMS + $CaCl_2$, and HDTMS + $NaHCO_3$ samples are similar, and there is no significant difference in the contact angle. Notably, the Si content in the HDTMS + $CaCl_2$ + $NaHCO_3$ sample was lower than HDTMS, HDTMS + $CaCl_2$, and HDTMS + $NaHCO_3$ samples. The reason being that its surface was covered with a large amount of $CaCO_3$, as the $CaCO_3$ surface contains few hydroxyl groups, it is difficult for silanes to adsorb via chemical bonding [38,39]. However, the HDTMS + $CaCl_2$ + $NaHCO_3$ sample exhibited the highest hydrophobicity, which is attributed to the fact that $CaCO_3$ altered the micro-nano structure of the sample surface, resulting in a significant increase in surface roughness (Fig. 3a). This suggests that the improvement in surface roughness, and in conjunction with HDTMS , can effectively enhance hydrophobicity.

4.2. Corrosion resistance

Water and Cl^- are often major factors contributing to the corrosion of steel [40–42]. As shown in Section 3.4 (Figs. 11, 12 and 13), the

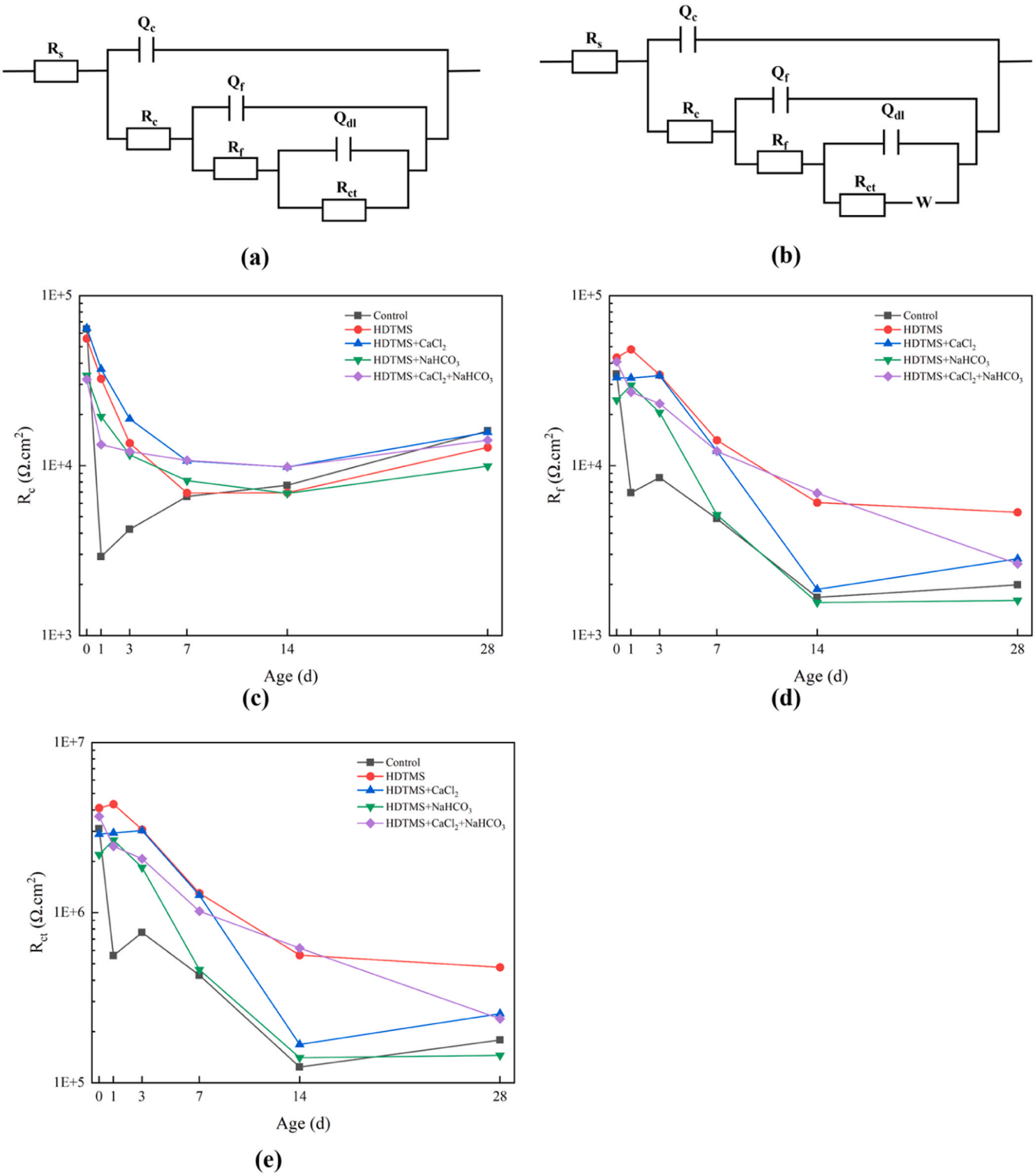

Fig. 12. Equivalent circuit modelling and fitting results of the EIS data: (a-b) equivalent circuit modelling; (c) R_c; (d) R_f; (e) R_{ct}.

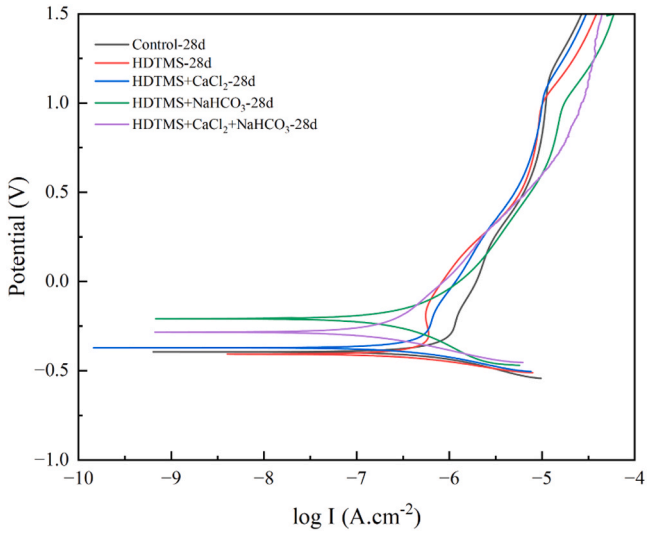

Fig. 13. Tafel result of different MKPC specimens at 28d.

Table 4
Electrochemical parameters obtained from tafel curves.

Sample	E'_{corr} (mV)	i_{corr} (μA/cm^2)
Control	−394.77	0.259
HDTMS	−407.06	0.151
HDTMS + $CaCl_2$	−371.63	0.144
HDTMS + $NaHCO_3$	−208.5	0.133
HDTMS + $CaCl_2$ + $NaHCO_3$	−283.81	0.073

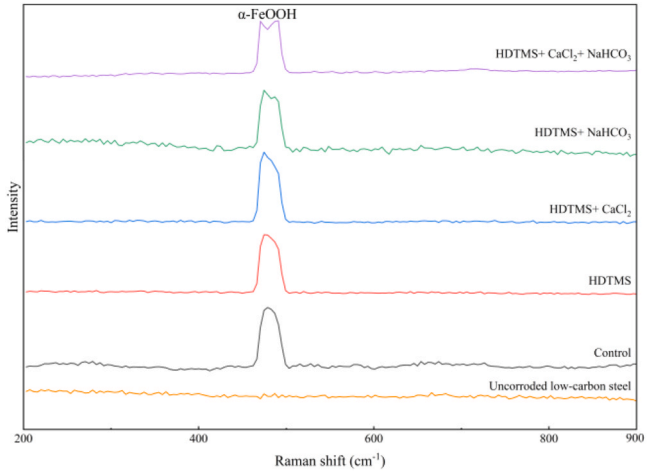

Fig. 14. Raman spectra of corrosion products formed on mild steel in different MKPC coating at 28d.

corrosion resistance of the MKPC coating following hydrophobic treatment is superior to the Control samples, particularly in the early stages. The mechanism is illustrated in Fig. 15, where hydrophobic treatment inhibits the penetration of water and Cl^- [15,43]. As the soak time increased, the hydrophobicity of the treated MKPC coating either decreased or was completely lost (Fig. 4), resulting in reduced resistance to the penetration of water and Cl^- into the coating, leading to a decline in corrosion resistance. However, during the soaking process, HDTMS remains exposed on the surface, thereby imparting low surface energy to the coating. Consequently, the i_{corr} value of the hydrophobic treatment samples remained lower than the Control (Fig. 13). Notably, hazenite continuously forms and fills the pores, making its structure denser (Fig. 8), which leads to an increase in the resistance of the MKPC coating in the later stages. Moreover, as shown in Fig. 13 and Table 4, the HDTMS + $CaCl_2$ + $NaHCO_3$ sample exhibited the best corrosion resistance at 28 d, with an i_{corr} value amounting to only 1/3 of the Control. This is due to the $CaCO_3$ adheres to the coating surface even after prolonged soaking and provides surface roughness, and its superior hydrophobicity at 28 d (Fig. 4). In addition, hazenite enhance the coating density (Fig. 8). The synergistic effect of these two factors effectively slows down the penetration of water and Cl^-, thereby improving the corrosion resistance of the substrate.

5. Conclusions

This study utilized SEM-EDS, contact angle measurement, XRD and Raman spectroscopy to investigate the effect of hydrophobic treatment on the properties of MKPC coatings. Furthermore, various electrochemical methods (including OCP, LPR, EIS and Tafel) were used to examine the corrosion resistance of low-carbon steel coated. Based on the results obtained, the following conclusions can be drawn:

(1) HDTMS can effectively improve the surface wettability of MKPC, and increasing the surface roughness further enhances hydrophobicity. By coating MKPC with HDTMS and creating micro-nano roughness through the formation of $CaCO_3$, a durable hydrophobic layer can establish. However, as the soaking time increases, K-struvite reacts with NaCl to gradually form hazenite, which coats the MKPC surface and leads to a reduction in hydrophobicity.
(2) As hazenite fills the pores, the porosity of MKPC decreases after soaking in a 3.5% NaCl solution. However, the reduction in porosity following hydrophobic treatment was less pronounced than the untreated sample. This is because hydrophobic treatment limits the contact between K-struvite and the NaCl in the solution, resulting in reduced formation of hazenite.
(3) Hydrophobic treatment of the MKPC coating significantly improves the corrosion resistance of low carbon steel. This is primarily due to the hydrophobic treatment effectively reduces water and Cl^- penetration. However, as the soaking time increases, the hydrophobicity of the coating decreases, leading to a decrease in corrosion resistance. Despite this decline, the corrosion current density in the HDTMS + $CaCl_2$ + $NaHCO_3$ sample remained three times lower than the untreated MKPC coating at 28 d.

CRediT authorship contribution statement

Tingyu Xiang: Writing – review & editing, Investigation, Data curation. **Xiong Xie:** Writing – original draft, Methodology, Investigation, Formal analysis, Data curation, Conceptualization. **Jinyang Jiang:** Supervision, Conceptualization. **Danqian Wang:** Writing – review & editing, Supervision, Funding acquisition, Conceptualization.

Declaration of Competing Interest

The authors declare that they have no known competing financial interests or personal relationships that could have appeared to influence the work reported in this paper.

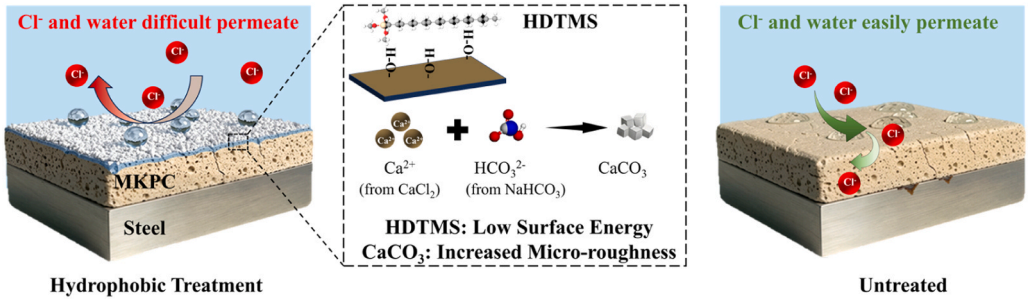

Fig. 15. Schematic illustration of the anti-corrosion mechanism of hydrophobic MKPC coating.

Acknowledgements

The authors would like to appreciate the financial support provided by the National Natural Science Foundation of China (NSFC) (Project No. 52578269) and Chongqing Construction Science and Technology Project (No. 2023–8–1).

Data availability

Data will be made available on request.

References

[1] C. Chiu, I. Liao, W. Tang, E. Yamaguchi, A quick estimation system of life-cycle costs including seismic and flood risks for steel bridges in Taipei City of Taiwan, Nat. Hazards 121 (1) (2025) 355–381, https://doi.org/10.1007/s11069-024-06812-w.
[2] A. Farahani, H. Taghaddos, M. Shekarchi, Prediction of long-term chloride diffusion in silica fume concrete in a marine environment, Cement andA.M.A. CJ. Dis. Child. Concr. Compos. 59 (2015) 10–17, https://doi.org/10.1016/j.cemconcomp.2015.03.006.
[3] B. Wang, K. Lu, C. Han, Q. Wu, Study on anti-corrosion performance of silica fume modified magnesium potassium phosphate cement-based coating on steel, Case Stud. Constr. Mater. 17 (2022), https://doi.org/10.1016/j.cscm.2022.e01467.
[4] M. Lei, Z. Liu, F. Wang, S. Hu, Development of Calcium Carbonate-Based Coatings by the Carbonation of Gamma-C2S (γ-C2S), Materials 15 (15) (2022), https://doi.org/10.3390/ma15155088.
[5] H. Moon, D. Shin, D. Choi, Evaluation of the durability of mortar and concrete applied with inorganic coating material and surface treatment system, Constr. Build. Mater. 21 (2) (2007) 362–369, https://doi.org/10.1016/j.conbuildmat.2005.08.012.
[6] G. Li, C. Guo, X. Gao, Y. Ji, O. Geng, Time dependence of carbonation resistance of concrete with organic film coatings, Constr. Build. Mater. 114 (2016) 269–275, https://doi.org/10.1016/j.conbuildmat.2016.03.198.
[7] D. Zhang, Y. Xian, Y. Ma, Z. Zhao, Y. Wu, L. Chen, Huidi Zhou, J. Chen, Research progress of inorganic phosphate-based compositecoatings in the surface protection fields((in Chinese), Surf. Technol. 49 (07) (2020) 68–75, https://doi.org/10.16490/j.cnki.issn.1001-3660.2020.07.009.
[8] B. Fang, Z. Hu, T. Shi, Y. Liu, X. Wang, D. Yang, K. Zhu, X. Zhao, Z. Zhao, Research progress on the properties and applications of magnesium phosphate cement, Ceram. Int. 49 (3) (2023) 4001–4016, https://doi.org/10.1016/j.ceramint.2022.11.078.
[9] H. Zhou, W. Deng, Q. Wang, R. Liang, D. Wang, Synergetic effect of passivity and hydrophobicity on the anticorrosion of magnesium phosphate cement-based coating on mild steel in Portland cement paste, Constr. Build. Mater. 492 (2025), https://doi.org/10.1016/j.conbuildmat.2025.143007.
[10] H. Tang, J. Qian, Z. Ji, X. Dai, Z. Li, The protective effect of magnesium phosphate cement on steel corrosion, Constr. Build. Mater. 255 (2020), https://doi.org/10.1016/j.conbuildmat.2020.119422.
[11] B. Yin, F. Fan, X. Hua, D. Qi, K. Han, D. Hou, Reinforced anticorrosive composite coating with mesh-brick structures and excellent air permeability on concrete, J. Build. Eng. 76 (2023), https://doi.org/10.1016/j.jobe.2023.107378.
[12] P. Yao, X. Lin, Y. Wu, T. Ji, Y. Liang, Influence of slag on water resistance of magnesium silicon potassium phosphate cement, J. Build. Eng. 97 (2024), https://doi.org/10.1016/j.jobe.2024.110862.
[13] X. Gan, H. Zhang, Z. Lu, K. Ma, X. Chen, L. Lu, L. Li, Effect of aluminum dihydrogen phosphate in enhancing mechanical properties and water resistance of magnesium phosphate cement, Cem. Concr. Res. 192 (2025), https://doi.org/10.1016/j.cemconres.2025.107849.
[14] L. Lv, P. Huang, L. Mo, M. Deng, J. Qian, A. Wang, Properties of magnesium potassium phosphate cement pastes exposed to water curing: a comparison study on the influences of fly ash and metakaolin, Constr. Build. Mater. 203 (2019) 589–600, https://doi.org/10.1016/j.conbuildmat.2019.01.134.
[15] Z. Feng, F. Wang, T. Xie, J. Ou, M. Xue, W. Li, Integral hydrophobic concrete without using silane, Constr. Build. Mater. 227 (2019), https://doi.org/10.1016/j.conbuildmat.2019.116678.
[16] Y. Zhang, L. Chen, Z. Liu, W. Li, S. Hong, G. Zhu, B. Dong, Manufacturing of integral hydrophobic concrete (IHC) using Pickering emulsion with limited effects on mechanical strength, Constr. Build. Mater. 312 (2021), https://doi.org/10.1016/j.conbuildmat.2021.125319.
[17] X. Quan, F. Zhou, C. Zhang, S. Ma, The effect of hydroxy silicone oil emulsion on the waterproof performance of cement, Materials 17 (12) (2024), https://doi.org/10.3390/ma17122797.
[18] L. Jiang, Z. Ma, Z. Gu, P. Shen, Y. Tao, W. Li, C. Poon, Impregnate Carbonation: CO2-guided in situ growth of robust superhydrophobic structures on concrete surfaces, Adv. Mater. 36 (40) (2024), https://doi.org/10.1002/adma.202405492.
[19] M. Grzegorczyk-Franczak, W. Andrzejuk, R. Hunek, G. Lagód, Effect of surface hydrophobization on the durability of concrete with cement Kiln Dust, Adv. Sci. Technol. -Res. J. 18 (3) (2024) 214–233, https://doi.org/10.12913/22998624/186212.
[20] F. Wang, H. Liu, J. Ou, W. Li, Fast fabrication of superhydrophobic surfaces on hardened cement paste using sodium laurate aqueous solution, Constr. Build. Mater. 278 (2021), https://doi.org/10.1016/j.conbuildmat.2021.122385.
[21] A. Arabzadeh, H. Ceylan, S. Kim, K. Gopalakrishnan, A. Sassani, S. Sundararajan, P. Taylor, Superhydrophobic coatings on Portland cement concrete surfaces, Constr. Build. Mater. 141 (2017) 393–401, https://doi.org/10.1016/j.conbuildmat.2017.03.012.
[22] W. She, X. Wang, C. Miao, Q. Zhang, Y. Zhang, J. Yang, J. Hong, Biomimetic superhydrophobic surface of concrete: topographic and chemical modification assembly by direct spray, Constr. Build. Mater. 181 (2018) 347–357, https://doi.org/10.1016/j.conbuildmat.2018.06.063.
[23] X. Liu, X. Liu, X. Zhang, L. Wang, One-step sprayable durable superhydrophobic coatings based on discrete epoxy binders: fabrication and performance, RSC Adv. 15 (54) (2025) 46391–46401, https://doi.org/10.1039/d5ra06946g.
[24] B. Xu, B. Lothenbach, Effect of seawater on hydration of magnesium potassium phosphate cements, Cem. Concr. Compos. 152 (2024), https://doi.org/10.1016/j.cemconcomp.2024.105639.
[25] J. Zhao, Study on NaCl Corrosion Mechanism of MagnesiumPhosphate Cement-Based Materials(M.S. thesis), University of Jinan, Jinan, China, 2024, https://doi.org/10.27166/d.cnki.gsdcc.2024.001226.
[26] J. Zhao, X. Gao, S. Chen, H. Lin, Z. Li, X. Lin, Hydrophobic or superhydrophobic modification of cement-based materials: A systematic review, Compos. Pt. B-Eng. 243 (2022), https://doi.org/10.1016/j.compositesb.2022.110104.
[27] W. Du, D. Wang, H. Yu, h Liluo, J. Luo, X. Deng, Weather resistance and failure mechanism of superhydrophobiccopper surface modified by mercaptans(in Chinese), Surf. Technol. 52 (11) (2023) 326–334, https://doi.org/10.16490/j.cnki.issn.1001-3660.2023.11.027.
[28] G. Hwang, K. Page, A. Patir, S. Nair, E. Allan, I. Parkin, The anti-biofouling properties of superhydrophobic surfaces are short-lived, ACS Nano 12 (6) (2018) 6050–6058, https://doi.org/10.1021/acsnano.8b02293.
[29] A. Baptiste, A. Gibaud, J. Bardeau, K. Wen, R. Maoz, J. Sagiv, B. Ocko, X-ray, micro-Raman, and infrared spectroscopy structural characterization of self-assembled multilayer silane films with variable numbers of stacked layers, Langmuir 18 (10) (2002) 3916–3922, https://doi.org/10.1021/la015572r.
[30] P. Wang, D. Long, K. Zhan, Y. Peng, Y. Wang, S. Liu, Monitoring CaCO3 content in recycled polypropylene with raman spectrometry, ACS Omega 9 (22) (2024) 23462–23467, https://doi.org/10.1021/acsomega.4c00414.
[31] D. Wang, Y. Yue, Z. Xie, T. Mi, S. Yang, C. McCague, J. Qian, Y. Bai, Chloride-induced depassivation and corrosion of mild steel in magnesium potassium phosphate cement, Corros. Sci. 206 (2022), https://doi.org/10.1016/j.corsci.2022.110482.
[32] X. Wang, A. Khaskhoussi, X. Hu, J. Yang, C. Shi, Performance of hydroxy-terminated polydimethylsiloxane-modified magnesium phosphate cement coatings on steel, Cem. Concr. Res. 207 (2026), https://doi.org/10.1016/j.cemconres.2026.108278.
[33] T. Mi, J. Wang, C. Mccague, Y. Bai, Application of Raman Spectroscopy in the study of the corrosion of steel reinforcement in concrete: a critical review, Cem. Concr. Compos. 143 (2023), https://doi.org/10.1016/j.cemconcomp.2023.105231.
[34] J. Liao, Y. Wang, Y. Wang, X. Lai, Preparation and evaluation of TA/APTES-HDTMS hydrophobic nanocomposite coating for enhancing corrosion resistance of

concrete, Constr. Build. Mater. 408 (2023), https://doi.org/10.1016/j.conbuildmat.2023.133792.
[35] Y. Zhao, S. Liu, J. Wang, R. Han, J. Tang, S. Zeng, Y. Zheng, Multifunctional self-cleaning coatings enhance superhydrophobicity and photocatalytic property of cement-based surface, J. Build. Eng. 118 (2026), https://doi.org/10.1016/j.jobe.2025.114967.
[36] X. Wang, A. Khaskhoussi, X. Hu, J. Yang, C. Shi, Surface energy and microstructural analyses of novel highly hydrophobic magnesium phosphate cement coatings, Cem. Concr. Compos. 163 (2025), https://doi.org/10.1016/j.cemconcomp.2025.106168.
[37] L. Jiang, H. Zheng, J. Xiong, Z. Fan, T. Shen, H. Xie, M. Chen, J. Li, Z. Gu, H. Li, W. Li, Fabrication of negative carbon superhydrophobic self-cleaning concrete coating: high added-value utilization of recycled powders, Cem. Concr. Compos. 136 (2023), https://doi.org/10.1016/j.cemconcomp.2022.104882.
[38] Z. Demjen, B. Pukanszky, E. Foldes, J. Nagy, Interaction of silane coupling agents with CaCO3, J. Colloid Interface Sci. 190 (2) (1997) 427–436, https://doi.org/10.1006/jcis.1997.4894.
[39] S. Kuriyavar, R. Vetrivel, S. Hegde, A. Ramaswamy, D. Chakrabarty, S. Mahapatra, Insights into the formation of hydroxyl ions in calcium carbonate: temperature dependent FTIR and molecular modelling studies, J. Mater. Chem. 10 (8) (2000) 1835–1840, https://doi.org/10.1039/b001837f.
[40] M. Ali, M. Shams, N. Bheel, A. Almaliki, A. Mahmoud, Y. Dodo, O. Benjeddou, A review on chloride induced corrosion in reinforced concrete structures: lab and in situ investigation, RSC Adv. 14 (50) (2024) 37252–37271, https://doi.org/10.1039/d4ra05506c.
[41] Y. Zhu, D. Macdonald, J. Yang, J. Qiu, G. Engelhardt, Corrosion of rebar in concrete. Part II: literature survey and statistical analysis of existing data on chloride threshold, Corros. Sci. 185 (2021), https://doi.org/10.1016/j.corsci.2021.109439.
[42] H. Takahashi, T. Kou, Y. Kato, E. Kato, Effect of water saturation in hardened mortar around a steel bar on corrosion considering exposure history, J. Build. Eng. 98 (2024), https://doi.org/10.1016/j.jobe.2024.111213.
[43] L. Qu, W. Song, Q. Wang, S. Xu, C. Hou, Effects of hydrophobic modified fly ash on resistance of chloride corrosion and water penetration of cement mortar in the early hydration stage, J. Build. Eng. 64 (2023), https://doi.org/10.1016/j.jobe.2022.105573.